Magnetic-Gradient-Free Two-Axis Control of a Valley Spin Qubit in math xmlns="http://www.w3.org/1998/Math/MathML" display="inline" overflow="scroll">msub>mi>Si/mi> mi>x/mi>/msub>msub>mi>Ge/mi>mrow>mn>1/mn>mo >−/mo>mi>x/mi>/mrow>/msub>/math>

Y.-Y. Liu, L.A. Orona, Samuel F. Neyens, E.R. MacQuarrie, M.A. Eriksson, and A. Yacoby

Phys. Rev. Applied **16**, 024029 — Published 17 August 2021

DOI: 10.1103/PhysRevApplied.16.024029

Magnetic-gradient-free two-axis control of a valley spin qubit in SiGe

Y.-Y. Liu,[1] L. A. Orona,[1] Samuel F. Neyens,[2] E. R. MacQuarrie,[2] M. A. Eriksson,[2] and A. Yacoby[1]

[1] *Department of Physics, Harvard University, Cambridge, Massachusetts 02138, USA*
[2] *University of Wisconsin-Madison, Madison, 53706, Wisconsin, USA*

(Dated: July 30, 2021)

Spins in SiGe quantum dots are promising candidates for quantum bits but are also challenging due to the valley degeneracy and weak spin-orbital coupling. In this work we demonstrate that valley states can serve as an asset that enables full two-axis control of a singlet-triplet qubit formed in a double quantum dot. We measure the valley spectrum in each dot using magnetic field spectroscopy of Zeeman split triplet states. We find a finite probability of valley states to flip during interdot transitions, which in turn provides a g-factor difference Δg between two dots. This Δg serves as an effective magnetic field gradient and allows for qubit rotations with a rate that increases linearly with an external magnetic field. We measured several interdot transitions and found that this valley introduced Δg is universal and electrically tunable. This could potentially simplify scaling up quantum information processing in the SiGe platform by removing the requirement for magnetic field gradients which are difficult to engineer.

INTRO

Quantum algorithms have been proposed to solve problems that are formidable for classical computers [1–4]. Electron spins confined to gate defined semiconductor quantum dots hold promise as quantum bits (qubits) due to the promise of long coherence times and the localized nature of their control, making them promising for scaling up to the large number of qubits required for real algorithms [5–8]. Single spin qubits have demonstrated high fidelity single qubit gates of 99.9% [9] and two qubit gates above 98% [10]. While the difficulty in addressing single spin quibts might be an obstacle for scaling up, singlet-triplet (ST) qubits have the advantage of having a Hamiltonian whose magnitude and direction can be electrically tuned from the exchange energy axis (J axis) to an additional control axis generated by a magnetic field gradient, ΔB_Z [11, 12]. This allows full two axis control without microwave drives.

Among all semiconductor platforms, silicon/silicon-germanium (Si/SiGe) is appealing because its weak nuclear spin background minimizes the decoherence caused by magnetic field fluctuations [8, 13]. Moreover, weak spin-orbit coupling further reduces the spin relaxation caused by charge fluctuation. This, however, is a double edged sword, because spin-orbital coupling can also be used for electrical spin control. In the absence of full electrical control, other works have used micromagnets placed near the qubit to create a local magnetic field gradient for an effective spin drive [7, 9, 12, 14]. Strong field gradients, however, are hard to create over large areas of the sample, posing challenges for scaling up this scheme. Another challenge is the valley degeneracy, which may also contribute to spin decoherence [15] and need to be removed by lattice strain and electrostatic confinement [16, 17]. This degeneracy can be measured using magneto spectroscopy, Hall Bar measurements and dispersive readout [16, 18, 19].

In this work we investigate a valley-assisted spin qubit formed in SiGe double quantum dots which does not require a magnetic field gradient to achieve two axis single qubit control. For interdot transitions where the electron number is (4n,4m) - (4n$\pm$1,4m$\mp$1), where n and m are integers, valley flipping is required for transitions between ground states in each dot. We perform magnetic field spectroscopy of Zeeman split triplet states (spin funnel measurement) [20] to map the valley spectrum in each dot and demonstrate that valley flipping at the interdot transition is allowed. This valley flip provides a g-factor difference Δg and generates a ΔB_Z rotation whose procession rate increases linearly with increasing magnetic field like other spin-orbital qubit [21, 22]. Importantly, this valley introduced Δg is also electric field dependent. The combined dependence on the magnetic and electrical fields enables a tunable ΔB_Z rotation. This could potentially simplify scaling up quantum information processing as it removes the need for fabricating micromagnets.

DEVICE AND METHOD

Figure 1(a) shows a scanning electron microscope image of a typical device that utilizes an overlap gate geometry to achieve quantum dot confinement [23]. The barrier gates, B, create potential barriers for controlling tunneling rates and plunger gates, P, select the charge state in each dot and tune their chemical potential. For this experiment, a double quantum dot (DQD, marked in yellow) is formed at the left two plunger gates P_1 to P_2, while P_3 to B_5 control the tunneling rate to a fermi sea. We also form a sensor dot (marked in orange) to perform charge detection and use RF-reflectometry for fast readout.

Figure. 1(b) demonstrates Pauli-blockade at the (4,0)-(3,1) transition, as required for forming a singlet-triplet qubit. The energy states of the DQD are dependent on

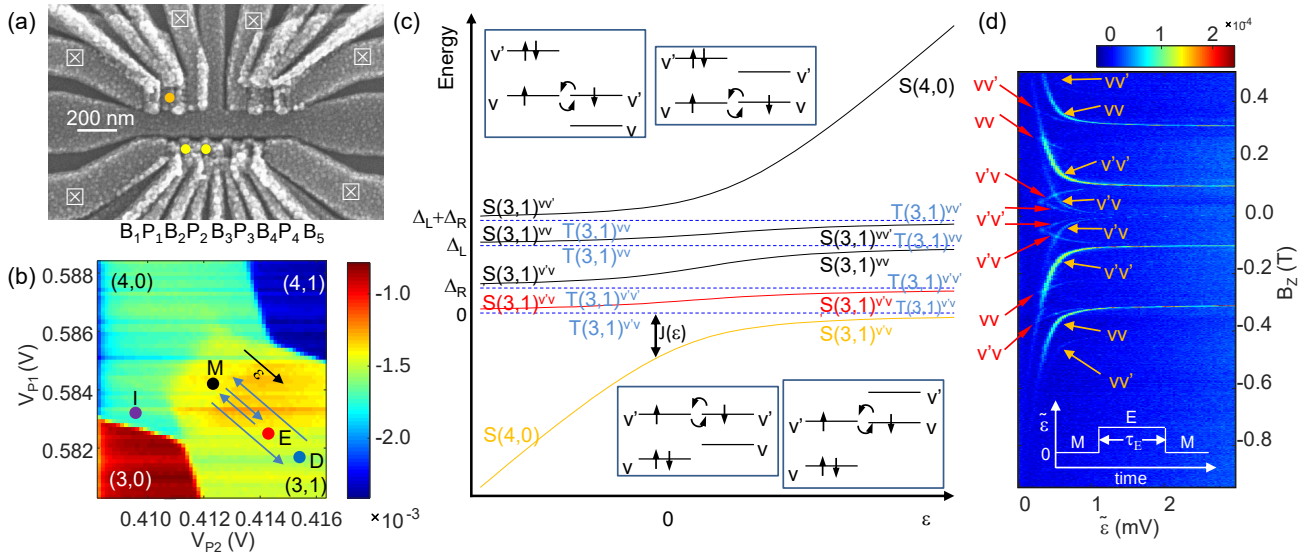

Figure 1. (a) SEM of an overlap style device. The DQD and sensor location are labeled as yellow and orange dots, respectively. (b) Charge stability diagram measured by performing charge readout as a function of plunger gate voltages after being prepared in a random (3,1) state. Spin blockade will keep triplets in configuration (3,1) in the bright area in the (4,0) region, giving rise to the readout position M. The position I is for the initialization of a singlet, position D is for minimizing interdot interaction and position E is for qubit operation. (c) Schematic level diagram as a function of ϵ with the singlet plotted as solid lines and triplets plotted as blue dashed lines. Inset: four possible (3,1) states interact with $S(4,0)$. (d) Spin funnel measurements that serve as valley spectroscopy. Two sets of curves are emphasized by the red and yellow arrows. The valley states of the triplets are labeled accordingly. Inset: pulse sequence.

which of the two valley eigenstates, v or v', the electrons occupy. Here we note that valley states v and v' can be different between dots, and thus there is no orthogonality. In the (4,0) charge state the four spin valley combinations of the ground orbital state are completely filled. The spin blockade region shown in Fig. 1(b) is cutoff by transitions into the excited orbital state, which is 200 μeV higher than the ground state and allows a triplet (4,0) states. This energy is large enough to be ignored in the spin dynamics discussed below.

The insets of Fig. 1(c) show the four possible (3,1) states that the ground (4,0) state can transition to without a spin flip. We use the notation $(3,1)^{\mathrm{ij}}$ where the superscript i represents the valley of the vacancy in the left dot and j represents the valley of the electron in the right dot. The ground (3,1) charge state is then $(3,1)^{\mathrm{v'v}}$. Assuming that the valley splitting in the left(right) dot is $\Delta_{L(R)}$, the three excited (3,1) valley states would be $(3,1)^{\mathrm{v'v'}}$, $(3,1)^{\mathrm{vv}}$ and $(3,1)^{\mathrm{vv'}}$ and are Δ_R, Δ_L and $\Delta_L + \Delta_R$ higher in energy compared to the $(3,1)^{\mathrm{v'v}}$ state. Singlet states $\mathrm{S}(3,1)^{\mathrm{v'v'}}$ and $\mathrm{S}(3,1)^{\mathrm{vv}}$ couple to S(4,0) without flipping the valley with a coupling rate t_c. $\mathrm{S}(3,1)^{\mathrm{v'v}}$ and $\mathrm{S}(3,1)^{\mathrm{vv'}}$ couple to S(4,0) while flipping the valley index at a different rate t_{c2}. The Hamiltonian of the singlet subspace in the basis of $\mathrm{S}(3,1)^{\mathrm{vv'}}$, $\mathrm{S}(3,1)^{\mathrm{vv}}$, $\mathrm{S}(3,1)^{\mathrm{v'v'}}$, $\mathrm{S}(3,1)^{\mathrm{v'v}}$ and S(4,0) can be written as

$$\begin{pmatrix} \Delta_R+\Delta_L & 0 & 0 & 0 & t_{c2} \\ 0 & \Delta_R & 0 & 0 & t_c \\ 0 & 0 & \Delta_L & 0 & t_c \\ 0 & 0 & 0 & 0 & t_{c2} \\ t_{c2} & t_c & t_c & t_{c2} & \epsilon \end{pmatrix} \quad (1)$$

where ϵ is the detuning between the chemical potentials of the ground (4,0) and (3,1) charge states.

Figure 1(c) plots the schematic energy diagram of all relevant states as a function of ϵ. The interdot coupling t_c, t_{c2} opens up the avoided crossing of all (4,0)-(3,1) singlet transitions, and leads to the hybridization of different $\mathrm{S}(3,1)^{\mathrm{ij}}$ singlets when $t_c, t_{c2} \gtrsim \Delta_{L(R)}$ as shown by the solid lines in Fig. 1(c). For all (3,1) triplet states, the Pauli blockade forbids the interdot transition and give rise to the energy levels as shown by the blue dashed lines. An external magnetic field B_z will further split the triplet states to T_+, T_0 and T_- that are separated by the Zeeman energy $E_Z = g\mu_B B_z$ (not shown in the figure).

VALLEY SPECTROSCOPY

Spin funnel measurements are standard technique that extracts the exchange energy $J(\epsilon)$ between the ground singlet and T_0, by detecting the S-T_+ degeneracy as a function of magnetic field B and ϵ. We first prepare the

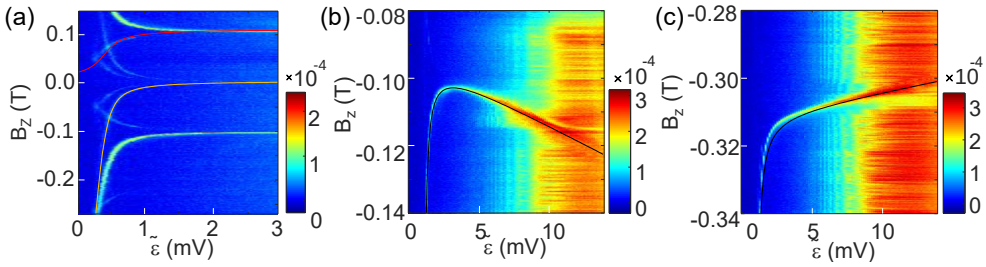

Figure 2. (a) Fit to the curves in Fig. 1(d). (b-c) Spin funnel measurements and fits that demonstrates the gate dependence of Δ_R (b) and Δ_L (c).

DQD in a singlet by loading the ground (4,0) state at I in Fig. 1(b) and then park at M. We then abruptly pulse the DQD to E and evolve for a time of $\tau_E = 1$ μs. Finally, we perform readout of the spin state at M. During the process we keep the pulse along the diagonal (ϵ) direction such that $\Delta V_{P2} = -\Delta V_{P1} = \tilde{\epsilon}$ with a lever arm that converts from gate potential to energy given by $\epsilon = 0.25\tilde{\epsilon}$ meV/mV. At a detuning where $E_Z = J(\epsilon)$, either a field gradient or spin-orbital coupling creates an interaction between the singlet state and the degenerate T_+ state and results in a finite probability P_T of flipping the state into a triplet state [11, 24, 25]. Fig. 1(d) demonstrates the data over $\tilde{\epsilon}$ = 0 - 3 mV and a magnetic field range B_z = -0.9 $\sim$ 0.5 T. A multitude of features symmetric in magnetic field are observed.

The orange arrows point to 4 pairs of curves where the position of the S-T+ transition is quickly changing with $\tilde{\epsilon}$. The orange v'v curve approaches zero field at large $\tilde{\epsilon}$ and maps out the the ground state singlet energy that is plotted as the orange line in Fig. 1(c). This results from the crossing of this ground singlet state and $T_+(3,1)^{\mathrm{v'v}}$. The other 3 pairs are parallel to the first pair and offset by 12 μeV, 33 μeV and 45 μeV, which corresponds to the intersection between the ground singlet and $T_+(3,1)^{\mathrm{v'v'}}$, $T_+(3,1)^{\mathrm{vv}}$ and $T_+(3,1)^{\mathrm{vv'}}$. From these observations we find valley splittings of 12 μeV and 33 μeV but we cannot tell which corresponds to Δ_L or Δ_R. We take $\Delta_L > \Delta_R$ for convenience in the following discussion.

Our experiments take place with an electron temperature of around 100 mK, which causes thermal excitation to the singlet state $S(3,1)^{\mathrm{v'v'}}$ with approximately a 10% probability at E. The energy spectrum of this state is plotted as the red curve in Fig. 1(c). We observe signatures of the degeneracy between this exited singlet state and the 4 triplet states as additional four pairs of curves indicated by the red arrows in Fig. 1(d). The red v'v' curves maps the degeneracy between $S(3,1)^{\mathrm{v'v'}}$ and $T_+(3,1)^{\mathrm{v'v'}}$. The crossing between $S(3,1)^{\mathrm{v'v'}}$ and $T_+(3,1)^{\mathrm{vv}}$ and $T_+(3,1)^{\mathrm{vv'}}$ leads to parallel curves with offsets of $\Delta_R - \Delta_L = 21\mu$eV and $\Delta_L = 33\mu$eV. The crossing between $S(3,1)^{\mathrm{v'v'}}$ and $T_-(3,1)^{\mathrm{v'v}}$ gives rise to red v'v curves with an offset of $\Delta_R = 12\mu$eV relative to the v'v' and a flipped direction of curve in response to the magnetic field because it is from the opposite Zeeman branch.

Figure 2(a) overlaps fits for the ground and first excited singlet energies (red and orange curve in Fig. 1(c)) with the data in Fig. 1(d). There is reasonable agreement between the model and data using the interdot coupling as the only free parameter with a best fit of $t_c = 15$ μeV. We further utilize this spectroscopy method to measure the gate dependence of $\Delta_{L(R)}$. Fig. 2(b) shows the second funnel in greater detail by reducing the range of B_z and enlarging the range of $\tilde{\epsilon}$. We fit the curve assuming $\Delta_R = \Delta_{R0} + \tilde{\epsilon}\Delta'_R$ and find $\Delta'_R = 0.3$ meV/V. Similarly we find $\Delta'_L = -0.09$ meV/V as shown in Fig. 2(c). This is comparable to results reported in previous works [15–17, 26].

The quantitative fitting indicates that all interdot transitions are allowed, whether they involve a flip between the valleys or not. The orange vv and v'v' curves are much brighter than orange v'v and vv' curves in Fig. 1(d), which suggests a larger P_T at these transitions. This is expected because flipping the singlet $S(4,0)$ to the $T_+(3,1)^{\mathrm{v'v'}}$ or $T_+(3,1)^{\mathrm{vv}}$ states does not require flipping the valley of the transitioning electron (Fig. 1(c) insets). This suggests that the valley states maybe similar between dots and a systematic quantitative study in P_T would help characterize the local valley states. Our spectroscopic technique is also applicable to valley qubits on arbitrary materials.

TUNABLE TWO AXIS CONTROL

Coherent qubit control is explored in the subspace spanned by the ground singlet and $T_0(3,1)^{\mathrm{v'v}}$. The Hamiltonian can be approximated by $H = J(\epsilon)\sigma_z + (g_L B_{zL} - g_R B_{zR})\mu_B \sigma_x$. Here $\sigma_{x,z}$ are the Pauli operators, $g_{L(R)}$ and $B_{zL(R)}$ are the g-factor and external field at left(right) dot. This system can achieve flexible two axis control as illustrated by the Bloch sphere in Fig. 3(a) [8, 12]. Rotation along the Z axis (J oration) can be performed near the interdot transition where $J(\epsilon)$ is large and $\{S, T_0\}$ are the eiganstate of the system Hamiltonian. X axis rotations (ΔB_z rotations) are achieved at

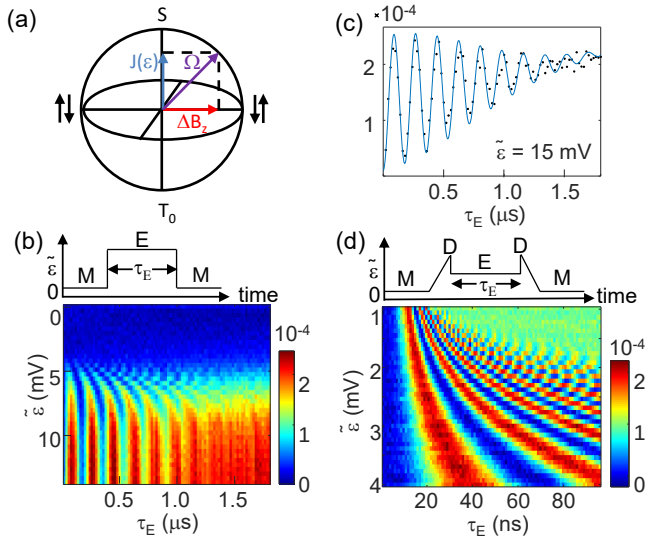

Figure 3. (a) The Bloch sphere for singlet-triplet qubit. (b) The charge readout as a function of $\tilde{\epsilon}$ and τ_E after the ΔB_Z rotation. Pulse sequences are plotted above the data. (c) A line cut of the data in panel (b) at $\tilde{\epsilon} = 15$ mV (black dot) and the fit (blue line) (d) The charge readout as a function of $\tilde{\epsilon}$ and τ_E after the ΔB_Z rotationand the J rotation. Pulse sequences are plotted above the data.

large ϵ where J(ϵ) is negligible and the energy splitting is set by $\mu_B(g_L B_{zL} - g_R B_{zR})$ and the eigenstates are $|\uparrow\downarrow\rangle$ and $|\downarrow\uparrow\rangle$ [11, 12].

We characterize the ΔB_Z rotations by initializing the system in $S(4,0)$ at M and then pulsing the DQD to spot E to turn off J, allowing the qubit to rotate around the ΔB_Z axis into superpositions of S and T_0. We then pulse back to M for readout [11, 12]. Figure 3(b) demonstrates charge readout as a function of evolve time τ_E and location ($\tilde{\epsilon}$) when we set the field $B_z = 1$ T. For $\tilde{\epsilon} > 10$ meV, we find an oscillation at a constant frequency $f_{\Delta \mathrm{Bz}} = 5.5$ MHz. In figure 3(c) we fit the oscillation at $\tilde{\epsilon} = 15$ mV to $A\cos(2\pi f_{\Delta \mathrm{Bz}}\tau_E)\exp(-(\tau_E/T_2^*)^2) + B\tau_E + C$. Here we find the coherence lifetime $T_2^* = 1$ μs. The constant $A = 1.2 \times 10^{-4}$ converts the spin probability to a charge readout voltage, $B = 5 \times 10^{-5}(\mu s)^{-1}$ reflects the readout position drift due to waveform distortions in the pulsing sequence and C is a background.

When $\tilde{\epsilon} < 10$ mV, the oscillation rate is larger than $f_{\Delta \mathrm{Bz}}$ and the amplitude is smaller, indicating a finite $J(\epsilon)$, which contributes to the rotation rate and shifts the angle from the ΔB_Z axis. J rotation can be characterized by a similar process by adding adiabatic ramping between M ($\tilde{\epsilon} = 0$) and D ($\tilde{\epsilon} = 15$ mV) to map S to $|\downarrow\uparrow\rangle$ and T_0 to $|\uparrow\downarrow\rangle$ [20]. The pulse sequence and result are presented in Fig. 3(d). For $1 < \tilde{\epsilon} < 4$ mV the rotation amplitude is constant and the rotation rate is strongly dependent on $\tilde{\epsilon}$. Here J is dominant, and the rotation rate is electrically tunable as expected.

We emphasize that no micromagnet or other external magnetic field gradient source was added to this device and thus $B_{zL} = B_{zL} = B_z$. To explore the mechanism we measure $f_{\Delta \mathrm{B_Z}}$ as a function of B_z. Figure 4(a) plots charge readout as a function of τ_E and B_z after a ΔB_Z rotation at $\tilde{\epsilon} = 10$ mV such that $J(\tilde{\epsilon})$ is negligible. The ΔB_Z rotation rate is then extracted and plotted as a function of field in Figure 4(b). The error bar $\delta f_{\Delta Bz}$ is the standard deviation of $f_{\Delta Bz}$ estimated from 10 measurements at the same magnetic field.

This result is consistent with a difference in the g factor of the two dots of around $\Delta g = 3.8 \times 10^{-4} = 0.02\% g$. We note that the two dots' ground states occupy different valley states and this Δg is consistent with the g factor difference between valleys as previously reported [27, 28]. In addition, we find $\delta f_{\Delta \mathrm{Bz}} \sim 0.5$ MHz for all field. Zeeman energy fluctuation is $h\delta f_{\Delta \mathrm{Bz}} \sim 2$ neV and is in good agreement with previous report [8]. This indicates that the major source of fluctuation is the background nuclei of 29Si in this isotopically nature silicon substrate.

This valley introduced Δg allows the rate of the ΔB_Z rotations to be tuned by an external magnetic field. We expect the ΔB_Z rotation rate would be 14 MHz at 3 T (beyond the current limit of our magnet), comparable to the field gradient generated by a micro-magnet [12]. This would potentially reduce design complexity for a large array of spin qubits because it eliminates the need for an artificially generated field gradient.

In order to verify the generality of this phenomena, we measured other (4n, 4m)-(4n±1, 4m∓1) transitions where the 4 valley spin states are all filled up in one dot and the relevant orbital of the other dot is empty. As in the case of (4,0)-(3,1), the ground states of the (4n, 4m) and (4n±1, 4m∓1) states occupy different valley states, which introduce a Δg to the singlet-triplet qubit Hamiltonian. Figure 4(c) labels these (4n, 4m)-(4n±1, 4m∓1) transitions with colored circles in the charge stability diagram. At the (1,3)-(0,4) transition, we measure $f_{\Delta \mathrm{Bz}}/B_z = 8$ MHz/T which is almost double the value for the (4,0)-(3,1) transition. This Δg could be electrical gate dependent.

To systematically study the gate dependence we focused on (5,3)-(4,4)-(3,5) transition where we can fix the barrier gate voltages and only change V_{P1} and V_{P2}. At the (5,3)-(4,4) we find $f_{\Delta \mathrm{Bz}}/B_z = 0$. Figure 4(d) demonstrates the ΔB_z rotation at the (4,4)-(3,5) transition using charge readout as a function of $\tilde{\epsilon}$ and τ_E. We find the rotation amplitude is maximized and the frequency increases with $\tilde{\epsilon}$ when $\tilde{\epsilon} > 8$ mV. This indicates $f_{\Delta \mathrm{Bz}}/B_z$ increases with $\tilde{\epsilon}$. At $\tilde{\epsilon} = 15$ mV $f_{\Delta \mathrm{Bz}}/B_z = 6$ MHz/T and at $\tilde{\epsilon} = 25$ mV, $f_{\Delta \mathrm{Bz}}/B_z$ has increased by 2 MHz/T. The gradient of Δg is 200 MHz/(T · V). The (5,3)-(4,4) transition is located at $\Delta V_{\mathrm{P1}} = -\Delta V_{\mathrm{P2}} > 40$ mV from the (4,4)-(3,5) transition. It is not surprising that $f_{\Delta \mathrm{Bz}}/B_z = 0$ at the (5,3)-(4,4) transition due to this rapid change in Δg.

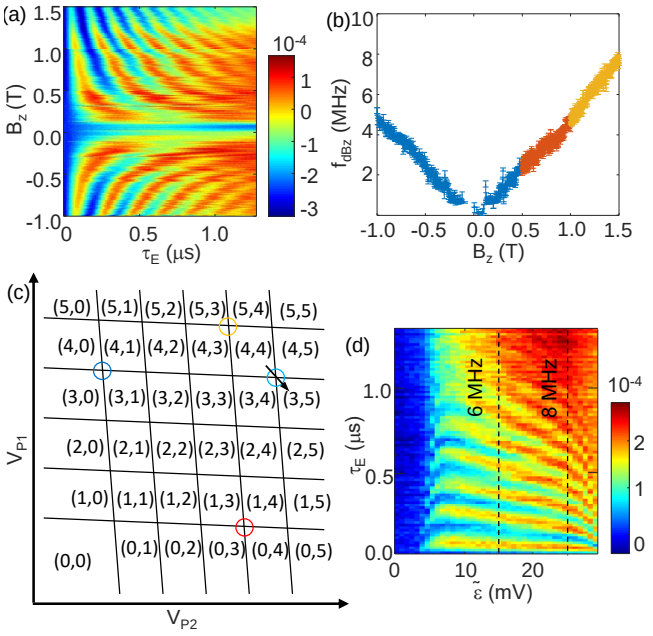

Figure 4. (a) The charge readout as a function of τ_E and B_z after a ΔB_Z rotation with $\tilde{\epsilon} = 10$ mV. Pulse used is the same as shown in Fig. 3(a). (b) $f_{\Delta \mathrm{bz}}$ as a function of B_z. (c) Schematic of a charge stability diagram. Colored circles labels the transitions that satisfy (4n, 4m)-(4n±1, 4m∓1). The arrow indicates the direction of ϵ. (d) The charge readout as a function of $\tilde{\epsilon}$ and τ_E after the ΔB_z rotation at (4,4) transition. Dashed lines indicates the range of $\tilde{\epsilon}$ that ΔB_z rotation is dominant and $f_{\Delta \mathrm{bz}}$ is labeled on top.

The gate dependence of the Δg could enable qubit operations that require fast changes in ΔB_z. The charge noise σ_ϵ introduces a fluctuation in the Zeeman energy gradient given by $\sigma_\epsilon \mu_B B_Z \epsilon \partial \Delta g / \partial \epsilon$. Typical charge noise that would cause charge dephasing rate $\sigma_\epsilon / h = 5$ MHz [19] would introduce dephasing rate of only 20–30 Hz along ΔB_z axis at $B_z = 1$ T. Compared to the field gradient generated by a micro-magnet, $f_{\Delta \mathrm{Bz}}$ by Δg can be arbitrarily high with increasing external field. The g factor difference between valleys has been explained by spin-orbital coupling in previous works [27, 28]. A gate dependent g factor has been predicted for SiGe [28] and observed in Si-MOS system [25, 29]. As with the valley splitting, a maximized Δg is expected for an atomically flat Si/SiGe interface and high external electrical field. We thus expect a potentially higher ΔB_z gate fidelity with better substrates and smaller QDs.

CONCLUSION

In this work we have investigated Si/SiGe DQD transitions where the electron number is (4n,4m)-(4n±1,4m∓1). The spin funnel measurements performed under these conditions introduce a technique for extracting the valley spectrum in each dot and prove that there is a finite probability of valley flips during interdot transitions. The ground state in each dot occupies a different valley state which provides a g-factor difference between the two charge states. This g-factor gradient generates a ΔB_z rotation that is linear to an external magnetic field and is also gate dependent. These two dependencies provide a tunable ΔB_z rotation that does not require a micro-magent. This would potentially simplify scaling up to large arrays of spin qubits for quantum information processing.

ACKNOWLEDGMENT

We acknowledge Lisa Edge from HRL Laboratories for the growth and distribution of the Si/SiGe heterostuctures that were used in this experiment. This work was sponsored by the Army Research Office (ARO), and was accomplished under Grant Number W911NF-17-1-0274 and W911NF-17-1-0202. We acknowledge the use of facilities supported by NSF through the UW-Madison MRSEC (DMR-1720415) and the MRI program (DMR-1625348). The views and conclusions contained in this document are those of the authors and should not be interpreted as representing the official policies, either expressed or implied, of the Army Research Office (ARO),or the U.S. Government. The U.S. Government is authorized to reproduce and distribute reprints for Government purposes notwithstanding any copyright notation herein.

[1] R. D. Somma, S. Boixo, H. Barnum, and E. Knill, Quantum simulations of classical annealing processes, Physical review letters **101**, 130504 (2008).
[2] G. Carleo and M. Troyer, Solving the quantum many-body problem with artificial neural networks, Science **355**, 602 (2017).
[3] A. Aspuru-Guzik, A. D. Dutoi, P. J. Love, and M. Head-Gordon, Simulated quantum computation of molecular energies, Science **309**, 1704 (2005).
[4] P. W. Shor, Polynomial-time algorithms for prime factorization and discrete logarithms on a quantum computer, SIAM review **41**, 303 (1999).
[5] V. N. Golovach, M. Borhani, and D. Loss, Electric-dipole-induced spin resonance in quantum dots, Phys. Rev. B **74**, 165319 (2006).
[6] J. J. Morton and B. W. Lovett, Hybrid Solid-State Qubits: The Powerful Role of Electron Spins, Annual Review of Condensed Matter Physics **2**, 189 (2011).
[7] L. Vandersypen, H. Bluhm, J. Clarke, A. Dzurak, R. Ishihara, A. Morello, D. Reilly, L. Schreiber, and M. Veldhorst, Interfacing spin qubits in quantum dots and donors—hot, dense, and coherent, npj Quantum Information **3**, 1 (2017).

[8] B. M. Maune, M. G. Borselli, B. Huang, T. D. Ladd, P. W. Deelman, K. S. Holabird, A. A. Kiselev, I. Alvarado-Rodriguez, R. S. Ross, A. E. Schmitz, et al., Coherent singlet-triplet oscillations in a silicon-based double quantum dot, Nature **481**, 344 (2012).

[9] K. Takeda, J. Yoneda, T. Otsuka, T. Nakajima, M. R. Delbecq, G. Allison, Y. Hoshi, N. Usami, K. M. Itoh, S. Oda, et al., Optimized electrical control of a Si/SiGe spin qubit in the presence of an induced frequency shift, npj Quantum Information **4**, 54 (2018).

[10] W. Huang, C. H. Yang, K. W. Chan, T. Tanttu, B. Hensen, R. C. C. Leon, M. A. Fogarty, J. C. C. Hwang, F. E. Hudson, K. M. Itoh, et al., Fidelity benchmarks for two-qubit gates in silicon, Nature **569**, 532 (2019).

[11] S. Foletti, H. Bluhm, D. Mahalu, V. Umansky, and A. Yacoby, Universal quantum control of two-electron spin quantum bits using dynamic nuclear polarization, Nature Physics **5**, 903 (2009).

[12] X. Wu, D. R. Ward, J. R. Prance, D. Kim, J. K. Gamble, R. T. Mohr, Z. Shi, D. E. Savage, M. G. Lagally, M. Friesen, et al., Two-axis control of a singlet-triplet qubit with an integrated micromagnet, Proc Natl Acad Sci USA **111**, 11938 (2014).

[13] R. Hanson, L. P. Kouwenhoven, J. R. Petta, S. Tarucha, and L. M. Vandersypen, Spins in few-electron quantum dots, Reviews of modern physics **79**, 1217 (2007).

[14] D. M. Zajac, A. J. Sigillito, M. Russ, F. Borjans, J. M. Taylor, G. Burkard, and J. R. Petta, Resonantly driven CNOT gate for electron spins, Science **359**, 439 (2018).

[15] C. H. Yang, A. Rossi, R. Ruskov, N. S. Lai, F. A. Mohiyaddin, S. Lee, C. Tahan, G. Klimeck, A. Morello, and A. S. Dzurak, Spin-valley lifetimes in a silicon quantum dot with tunable valley splitting, Nature Communications **4**, 2069 (2013).

[16] S. Goswami, K. A. Slinker, M. Friesen, L. M. McGuire, J. L. Truitt, C. Tahan, L. J. Klein, J. O. Chu, P. M. Mooney, D. W. van der Weide, et al., Controllable valley splitting in silicon quantum devices, Nature Physics **3**, 41 (2007).

[17] M. Friesen and S. N. Coppersmith, Theory of valley-orbit coupling in a Si/SiGe quantum dot, Phys. Rev. B **81**, 115324 (2010).

[18] M. G. Borselli, R. S. Ross, A. A. Kiselev, E. T. Croke, K. S. Holabird, P. W. Deelman, L. D. Warren, I. Alvarado-Rodriguez, I. Milosavljevic, F. C. Ku, et al., Measurement of valley splitting in high-symmetry Si/SiGe quantum dots, Appl. Phys. Lett. **98**, 123118 (2011).

[19] X. Mi, C. G. Péterfalvi, G. Burkard, and J. R. Petta, High-Resolution Valley Spectroscopy of Si Quantum Dots, Phys. Rev. Lett. **119**, 176803 (2017).

[20] J. R. Petta, A. C. Johnson, C. M. Marcus, M. P. Hanson, and A. C. Gossard, Manipulation of a Single Charge in a Double Quantum Dot, Phys. Rev. Lett. **93**, 186802 (2004).

[21] R. M. Jock, N. T. Jacobson, P. Harvey-Collard, A. M. Mounce, V. Srinivasa, D. R. Ward, J. Anderson, R. Manginell, J. R. Wendt, M. Rudolph, et al., A silicon metal-oxide-semiconductor electron spin-orbit qubit, Nature Communications **9**, 1768 (2018).

[22] D. Jirovec, A. Hofmann, A. Ballabio, P. M. Mutter, G. Tavani, M. Botifoll, A. Crippa, J. Kukucka, O. Sagi, F. Martins, et al., A singlet triplet hole spin qubit in planar Ge (2020), 2011.13755.

[23] D. M. Zajac, T. M. Hazard, X. Mi, K. Wang, and J. R. Petta, A reconfigurable gate architecture for Si/SiGe quantum dots, Appl. Phys. Lett. **106**, 223507 (2015).

[24] J. R. Petta, J. M. Taylor, A. C. Johnson, A. Yacoby, M. D. Lukin, C. M. Marcus, M. P. Hanson, and A. C. Gossard, Dynamic Nuclear Polarization with Single Electron Spins, Phys. Rev. Lett. **100**, 067601 (2008).

[25] P. Harvey-Collard, R. M. Jock, N. T. Jacobson, A. D. Baczewski, A. M. Mounce, M. J. Curry, D. R. Ward, J. M. Anderson, R. P. Manginell, J. R. Wendt, et al., in *2017 IEEE International Electron Devices Meeting (IEDM)* (2017), pp. 36.5.1–36.5.4.

[26] A. Hollmann, T. Struck, V. Langrock, A. Schmidbauer, F. Schauer, T. Leonhardt, K. Sawano, H. Riemann, N. V. Abrosimov, D. Bougeard, et al., Large, Tunable Valley Splitting and Single-Spin Relaxation Mechanisms in a Si/Si_xGe_{1-x} Quantum Dot, Phys. Rev. Applied **13**, 034068 (2020).

[27] E. Kawakami, P. Scarlino, D. R. Ward, F. R. Braakman, D. E. Savage, M. G. Lagally, M. Friesen, S. N. Coppersmith, M. A. Eriksson, and L. M. K. Vandersypen, Electrical control of a long-lived spin qubit in a Si/SiGe quantum dot, Nature Nanotechnology **9**, 666 (2014).

[28] R. Ferdous, E. Kawakami, P. Scarlino, M. P. Nowak, D. R. Ward, D. E. Savage, M. G. Lagally, S. N. Coppersmith, M. Friesen, M. A. Eriksson, et al., Valley dependent anisotropic spin splitting in silicon quantum dots, npj Quantum Information **4**, 26 (2018).

[29] M. Veldhorst, R. Ruskov, C. H. Yang, J. C. C. Hwang, F. E. Hudson, M. E. Flatté, C. Tahan, K. M. Itoh, A. Morello, and A. S. Dzurak, Spin-orbit coupling and operation of multivalley spin qubits, Phys. Rev. B **92**, 201401 (2015).